RESEARCH AND EXPERIMENT OF RAPID DISENGAGEMENT SYSTEM FOR KELP SEEDLING ROPES BASED ON A LOCKING DEVICE

/

基于锁扣结构的海带苗绳快速脱扣技术研究与试验

Zehao ZHA[1)], Jianning YIN[1)], Qiming YU[1)], Pengxuan GUAN[1)], Yipeng CUI[1)], Xian WANG[1)], Xinxin WANG[1)], Tongfei SHENG[2)], Duanyang GENG[1*)]

[1)] School of Agricultural Engineering and Food Science, Shandong University of Technology, Zibo 255000, China

[2)] Weihai Renhe Electromechanical Co., Ltd., Weihai Shandong 264200, China

[*)] Corresponding authors. Tel.: +86 13668641238; E-mail address: dygxt@sdut.edu.cn (D.Y. Geng).

DOI: https://doi.org/10.35633/inmateh-76-110

Keywords: *kelp harvesting, locking device, disengagement device, seedling rope disengagement, Programmable Logic Controller (PLC) control*

ABSTRACT

In China's algae farming, ropes are widely used for seedling cultivation and suspension, requiring fast and reliable uncoupling during harvest. However, current kelp harvesting faces issues like complex rope connections, low unlocking efficiency, and poor reusability. To address this, a PLC-controlled rapid disengagement system was developed. The proposed system employs a button with self-locking functionality, coupled with a magnetically controlled disengagement device, to achieve automated unfastening of seedling ropes without damaging the suspension rope. The paper presents the components and operating principle of the locking device. To address the force characteristics of the seedling rope during the disengagement process, a dual-fingered pusher configuration was designed. The use of an involute trajectory enabled stable extraction of the rope from the locking groove. A Delta PLC was employed as the central controller, and an execution system comprising of an electric push rod, proximity sensors, magnetic adsorption module, and rope-pulling motor was developed to achieve automated control of lock correction, magnetic positioning, unlocking, and rope disengagement. Experimental results indicated that the system achieved the highest disengagement success rate of 96.67% when the guiding slot clearance was 14 mm, the haulage rope speed was 40 mm/s, and the pusher length was 45 mm, demonstrating stable and reliable device performance.

摘 要

在我国海藻养殖过程中，绳索广泛应用于苗体的吊挂和培育，收获阶段对苗绳与绠绳的快速可靠脱扣提出了更高要求。然而，当前海带收获普遍存在连接方式复杂、解扣效率低、结构不可重复使用等问题。为此，本文开发了一种基于 PLC 控制的海带苗绳快速脱扣系统。该系统采用具有自锁功能的按钮结构，结合磁控脱扣装置，实现苗绳在不损伤吊绳的前提下自动解扣。文中介绍了锁扣结构的组成与工作原理。针对苗绳在脱扣过程中的受力特性，设计了双拨指结构，并利用渐开线轨迹实现苗绳从挂接槽中的稳定拨出。控制系统以台达 PLC 为核心，配套电动推杆、接近传感器、磁吸模块及拨绳电机，实现了锁扣矫正、磁吸定位、解锁与苗绳脱出的全流程自动控制。试验结果表明，当导向槽间隙为 14 mm、绠绳行进速度为 40 mm/s、拨指长度为 45 mm 时，系统脱扣成功率最高可达 96.67%，装置运行稳定可靠。

INTRODUCTION

Kelp is a type of large brown seaweed that primarily grows in cold marine environments and represents one of the most important economic algal resources *(Branch et al. 2023; Forbes et al. 2022; Grebe et al. 2019)*. In recent years, with the rapid development of the kelp industry, the scale of aquaculture has expanded annually, positioning China as the global leader in kelp production *(Hewei et al., 2020; Zimin et al., 2021)*. According to statistics, China's total kelp output reached 1.6 million tonnes in 2022, accounting for 89.4% of the global production, which presents significant technical challenges for kelp cultivation and harvesting *(Zimin et al. 2023)*. Currently, kelp harvesting largely depends on manual labor or semi-mechanized equipment *(Mac Monagail et al., 2017; Tullberg et al., 2022)*. Particularly, the connection and disconnection between seedling ropes and haulage or suspension ropes are commonly performed through manual knotting and unfastening. This process is not only labor-intensive, time-consuming, and inefficient, but also poses safety risks *(Mac Monagail et al., 2017; Yongming et al., 2020)*, making it inadequate for meeting the development needs of the modern kelp industry *(Bak et al., 2018)*. Therefore, the development of a rapid disengagement system for seedling ropes from haulage and suspension ropes is crucial to addressing these challenges.

Extensive research has been conducted by both domestic and international scholars to address the technical challenges associated with mechanizing kelp harvesting. For instance, in Norway was developed an articulated crane system for the efficient harvesting of wild kelp *(Peteiro et al., 2016; Vea and Ask, 2010)*, which is suitable only for naturally grown kelp without seedling ropes and thus is ineffective for China's flat-raft kelp cultivation model *(Zongyu et al., 2018)*. In China, various kelp harvesting machines have also been developed, such as rope-hook integrated harvesters, yet the separation of seedling ropes from haulage ropes still relies entirely on manual operation. Jiang Tao's team developed an automatic towing-type kelp harvesting vessel and a kelp harvest and transfer device *(Tao et al., 2020; Tao et al., 2022; Yongming et al., 2018)*, but it is poorly compatible with standard flat-raft cultivation systems. Liu Hewei and colleagues designed a bionic kelp harvester based on the motion analysis of manual harvesting *(Hewei and Bin, 2020)*. These devices enable large-scale kelp harvesting, but still face issues in practice, such as difficulties in separating seedling or suspension ropes from haulage ropes and unstable operational performance. Clearly, with the rapid advancement of automation and intelligent technologies, developing an integrated automated and mechanized rapid unlocking system is crucial for the efficient separation of seedling and haulage ropes.

In light of these challenges, this study aims to develop a rapid disengagement system for seedling ropes to improve the efficiency, automation, and reliability of kelp harvesting. The proposed solution focuses on enabling automated separation between seedling and haulage ropes under complex working conditions, ensuring operational stability while reducing labor intensity and time consumption. By addressing the bottleneck of manual disengagement, the research provides a practical foundation for the mechanization and intelligent transformation of kelp harvesting processes.

MATERIALS AND METHODS

Overall structure and working principle

As shown in Figure 1, the test platform for the rapid disengagement of kelp seedling ropes mainly consists of a motor, flared guiding slot, electric push rod, magnet, proximity sensor, and control unit.

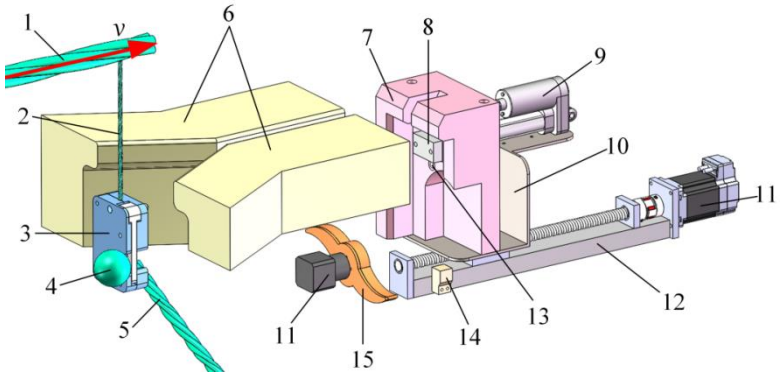

Fig. 1 - Schematic diagram of the complete machine structure

1 - Haulage rope; 2 - Suspension rope; 3 - Locking device; 4 - Seedling rope knot; 5 - Seedling rope; 6 - Flared guiding slot; 7 - Blocking plate; 8 - Magnet; 9 - Electric push rod; 10 - Supporting plate; 11 - Stepper motor; 12 - Lead screw; 13 - Proximity sensor; 14 - Metal sensing switch; 15 - Pusher

During the simulation operation, the winch system drives the haulage rope forward, the lead screw moves the blocking plate to the initial position, and the locking device connected to the haulage rope enters the flared guiding slot. It is then guided into a slot of equal width to the quick-locking device under the constraint of the flared slot. Since both ends of the seedling rope are connected to the suspension rope via locking devices, its posture can only be maintained with the contact point oriented forward. This ensures that the locking device enters the disengagement region on the blocking plate with the same posture. When the locking device enters the effective magnetic range, it is attracted to the blocking plate aligned with the electric push rod. The electric push rod then drives the locking device toward the blocking plate, and upon contact, the blocking plate applies pressure to the button on the locking device, triggering the release of the internal locking device and completing the unlocking operation. Once the locking device engages the proximity sensor, the motor drives the pusher to rotate, dislodging the knotted seedling rope from the unlocked locking device. After disengagement, the lead screw retracts the blocking plate, releasing the locking device from the magnetic holding area and restoring its freedom of movement. Then, the haulage rope moves diagonally upward, carrying the disengaged locking device away from the device, thus preparing space for the next disengagement operation.

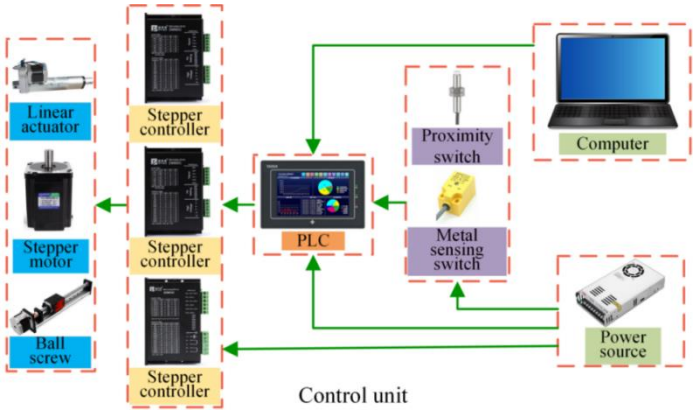

Fig. 2 - Control unit of the disengagement device

Study of key components and mechanisms

Determination of the locking device

To achieve rapid disengagement of the seedling rope from the haulage rope, a quick-release structure, as illustrated in Figure 3, was developed. It mainly consists of a housing, button, torsion spring, latch, and iron block. The locking device functions through a button-triggered quick-release mechanism. When external pressure is applied to the button, its internal protrusion disengages from the limit groove in the housing. This disengagement removes the mechanical constraint on the latch, allowing it to rotate under the restoring force of the torsion spring. As the latch opens, the seedling rope locking channel is released, enabling the pusher to separate the rope from the haulage system. It can significantly improve the efficiency of separating the seedling rope from the haulage rope.

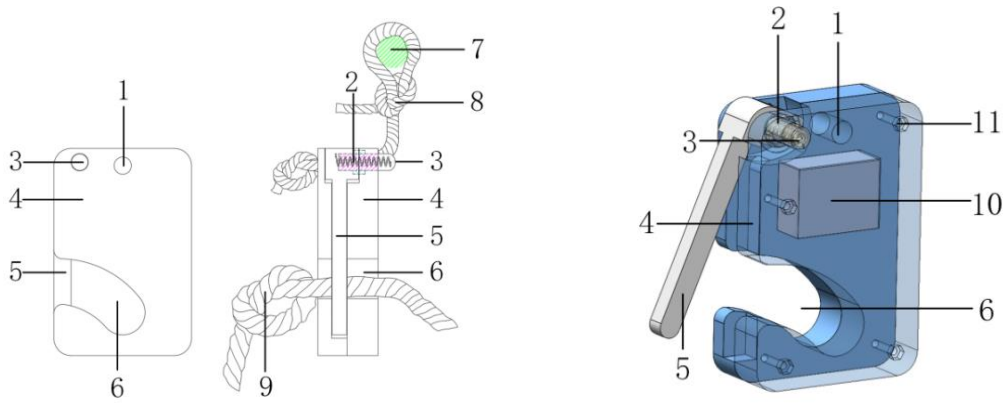

(a) Schematic diagram of the planar structure (b) Schematic diagram of the 3D structure

Fig. 3 - Structural diagram of the locking device for kelp seedling ropes

1 - Suspension rope connection hole; 2 - Torsion spring; 3 - Button; 4 - Housing; 5 - Latch; 6 - Seedling rope locking groove; 7 - Haulage rope; 8 - Suspension rope; 9 - Seedling rope; 10 - Iron block; 11 - Housing mounting hole

Analysis of torsion spring torque and button loading

From the above structure, the torsion spring is the key to the instantaneous opening of the latch, as shown in Figure 4 and Figure 5. During operation, when the locking structure moves to the position of the magnet-equipped blocking plate, it is firmly attracted to the plate by magnetic force. The plate then depresses the button on the locking structure, driving the internal protrusion out of the button limiting slot in the housing. The latch thereby loses the constraint of the protrusion and, under the torque of the torsion spring, instantly rotates by an angle, thus opening the seedling-rope engagement channel.

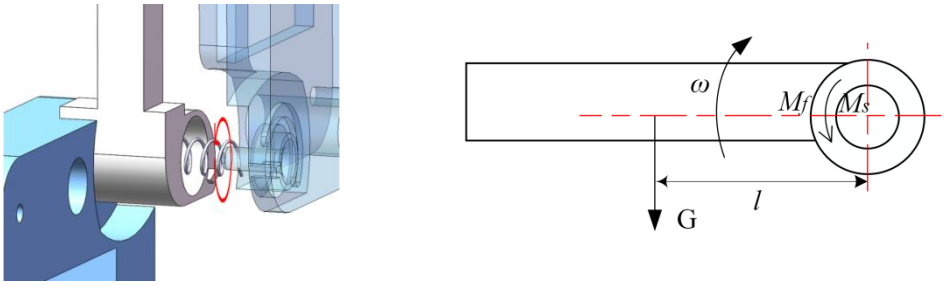

(a) Pre-rotational installation of torsion spring (b) Simplified force diagram of the latch

Fig. 4 - Diagram of torsion spring installation and latch force analysis

Evidently, the torsional moment of the torsion spring is critical to reliably opening the seedling-rope engagement channel. To ensure the spring has sufficient capacity to actuate the latch, a torque analysis of the latch is conducted:

$$\begin{cases} M_g = Gl \\ M_s = k\theta \\ M_s = M_g + M_f \end{cases} \quad (1)$$

where: M_g is the gravitational torque caused by its own weight, Nm; G is the weight of the latch, N; l is the distance from the latch centroid to the rotation center, m; M_s is the torsion spring moment, Nm; k is the torsional stiffness of the torsion spring, N·m/(°); θ is the torsional angle of the spring, (°); M_f is the frictional moment at the latch ends, Nm.

During rotation, only the two end faces of the latch seat contact the housing, so friction and a corresponding frictional torque act at these faces. To ensure that the latch opens stably and holds its position—and to avoid re-closure even in the event of a sudden torsion-spring failure—the minimum frictional torque between the latch and the housing should equal the gravitational torque of the latch; thus, we have:

$$M_f = M_g \quad (2)$$

To compute the minimum torsion-spring torque, substituting Equation (2) into Equation (1) yields the spring torque as:

$$M_s = M_g + M_f = 2M_g \quad (3)$$

Considering system reliability and the influence of the operating environment, we set:

$$M_s = n(M_g + M_f) = 2nM_g \quad (4)$$

where: n is the safety factor for system operation, and in this study, considering both the load magnitude and the working environment, n is set to 2.5. Thus, we have:

$$M_s = k\theta = 5M_g \quad (5)$$

According to the torque calculation formula of the torsion spring, it results:

$$k = \frac{5Gl}{\theta} \quad (6)$$

For simplicity, it is assumed that once the latch-locking button is released, the latch can rotate by 90°. Clearly, the longer the latch, the greater its weight and the larger the required torsion-spring stiffness coefficient k; conversely, a shorter latch requires a smaller stiffness k.

The detailed structure of the button is shown in Figure 5(a). The button is the key component for unlocking the locking structure. Its core function is to apply pressure to the button, causing the protrusion on it to disengage from the button limiting slot inside the locking structure housing, allowing the torsion spring to release its rotational force, transferring the force to the button. The button then drives the latch to rotate, opening the locking structure. As shown in Figure 5(b), the button is mainly influenced by the pressure from the blocking plate, its own weight, and the torsion spring moment.

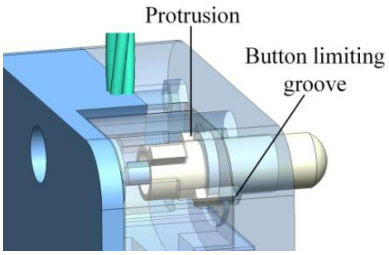

(a) Structural diagram of the button

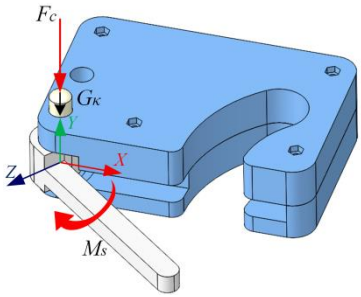

(b) Force analysis diagram of the button

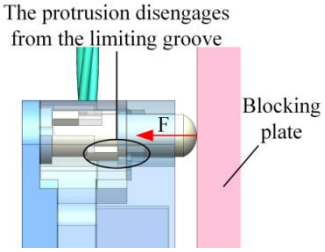

(c) The blocking plate applying pressure to the button

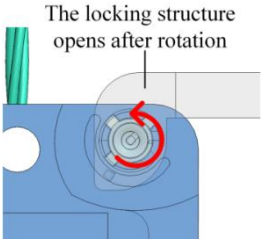

(d) Rotation to open after disengaging from the limiting groove

Fig. 5 - Schematic diagram of the button structure and unlocking process

As shown in Figure 5(c), when the button contacts the blocking plate, it is subjected to a compressive load determined by the contact force between the button and the plate. Thus:

$$F_c = k_\delta \cdot \Delta x \tag{7}$$

where: F_c is the compressive force applied by the blocking plate to the button, N; k_δ is the contact stiffness coefficient, N/m; Δx is the displacement of the button under the applied load, m.

The contact stiffness is:

$$k_\delta = \frac{G_\delta d^4}{8D^3\eta} \tag{8}$$

where:

G_δ is the shear modulus of the material, MPa; d is the spring wire diameter, m; D is the mean coil diameter, m; and η is the number of active turns.

Since the button's position within the button limiting slot is influenced by external forces, the vertical force on the button can be estimated as:

$$F_0 = \frac{G_\delta d^4}{8D^3\eta} \cdot \Delta x + G_\kappa \tag{9}$$

where:

F_0 is the force exerted by the button in the vertical direction, N; G_κ is the self-gravity of the button, N.

Study on the Rapid Disengagement Device

Study on the Flared Guiding Slot

During the kelp harvesting process, the seedling rope is kept under tension with the locking device due to the weight of the kelp, which causes the locking device to assume a tilted angle. To ensure a smooth transition of the locking device from its inclined initial posture to the vertical constrained disengagement position, the flared guiding slot must have continuous posture adjustment capability. Therefore, the inner surface of the flared guiding slot is designed as a helical surface with spatially varying geometry, incorporating a bivariate design that controls both angular orientation and radial offset, to enhance the stability of lock insertion and the precision of disengagement.

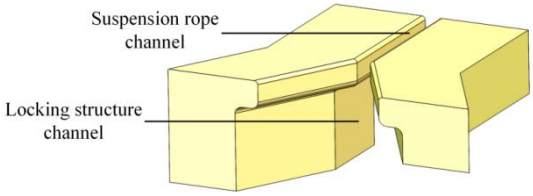

Fig. 6 - Structure of the flared guiding slot

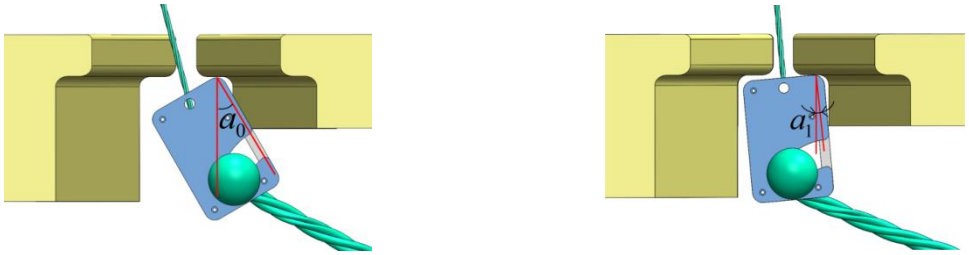

(a) Initial angle of the locking device

(b) Angle of the locking device after being guided through the constricted slot

Fig. 7 - Comparison of the locking device before and after posture adjustment in the guiding slot

Having L as the length of the guiding slot, and defining a parametric surface over u that belongs to $[0, L]$, then a helical surface with simultaneous variation in radial distance and angular orientation is obtained.

$$\begin{cases} x(u,v) = u \\ y(u,v) = r(u)\cos(\theta(u)) + v\cdot\cos(\theta(u)) \\ z(u,v) = r(u)\sin(\theta(u)) + v\cdot\sin(\theta(u)) \end{cases} \quad (10)$$

where: u is the advancement coordinate of the locking device along the guiding slot, v belongs to $[-w/2, w/2]$ is the variable along the width direction of the guiding slot wall surface, $r(u)$ is the radial offset function between the guiding slot wall and the central axis, $\theta(u)$ is the angular orientation function of the posture, w is the maximum lateral dimension of the locking device.

To achieve a smooth transition of the angle from a_0 to a_1 (see fig.7), a fifth-order Bezier function is introduced.

$$\theta(u) = \sum_{i=0}^{5} B_{i,5}(t)\cdot\theta_i, t = \frac{u}{L} \quad (11)$$

where: θ_i are the six control angle points of the fifth-order Bezier curve, The variable t ranges from [0, 1] and controls the distribution of points along the curve between the given control points, $B_{i,5}(t)$ is the Bernstein basis function, defined as:

$$B_{i,5}(t) = \binom{5}{i}(1-t)^{5-i}t^i \quad (12)$$

Similarly, to achieve a gradually narrowing design of the guiding slot width, the radial offset function $r(u)$ is expressed using a second-order Bezier curve.

$$r(u) = (1-t)^2 r_0 + 2(1-t)tr_m + t^2 r_1, t = \frac{u}{L} \quad (13)$$

where: r_0 is the radius at the entrance of the guiding slot, r_m is the radius at the middle section of the guiding slot, r_1 is the radius at the end of the guiding slot.

Study on the Pusher Configuration and Motor Selection

The pusher configuration is one of the key components of the entire disengagement device, and its function is to ensure that the seedling rope can be smoothly disengaged from the locking device, thereby enabling the automated unlocking process *(Min et al., 2023; Yiren et al., 2021)*. To ensure the operational stability of the pusher configuration, a dual-pusher design was adopted.

To ensure that the motion trajectory of the pusher matches the trajectory of the locking groove on the locking device, the design of the pusher configuration must incorporate the involute curve equation. The involute equation can be expressed as:

$$\begin{cases} x = r(\theta - \sin\theta) \\ y = r(1 - \cos\theta) \end{cases} \tag{14}$$

where: r is the radius of the pusher, θ is the rotation angle of the pusher.

By optimizing the involute curve, the trajectory of the pusher can be made consistent with that of the locking groove on the locking device, effectively avoiding rope jamming caused by trajectory mismatch.

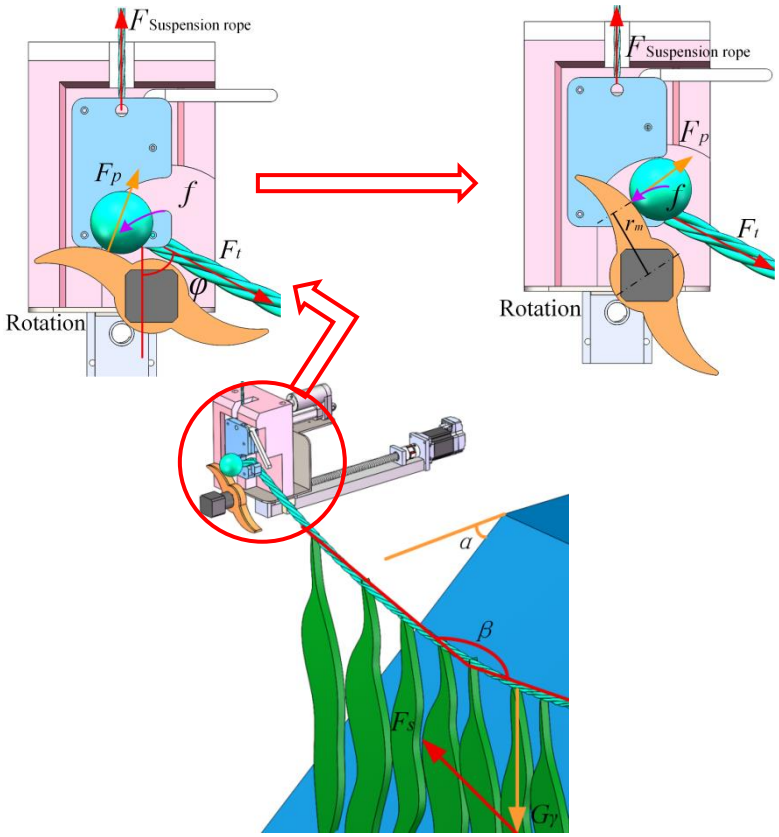

Fig. 8 - Schematic diagram of the pusher configuration and force analysis

After the locking device is unlocked, the pusher, driven by the motor, performs the rope disengagement operation. For successful disengagement, the pushing force applied by the pusher must be greater than the sum of the tensile force in the rope and the frictional force between the rope and the locking groove:

$$F_p > F_t + f \tag{15}$$

where: F_p is the pushing force applied by the pusher, N; F_t is the tensile force in the rope, N; f is the frictional force between the rope and the locking groove, N.

During the unlocking process, the pusher must overcome the combined weight of the seedling rope and kelp, as well as the frictional force between the seedling rope and the locking groove, to ensure successful disengagement of the seedling rope. During harvesting, the kelp is first lifted onto the hauling platform before rope disengagement is performed, thus, the platform provides partial support to the kelp, and the rope disengagement is carried out simultaneously by rapid disengagement devices on both sides, so the load should be considered as equally distributed. When the kelp contacts the hauling platform, it is saturated with water and tends to adhere to the surface, and the effect of friction is neglected in this analysis. The conveyor belt exerts a supporting force on the kelp, which is related to the installation inclination angle α of the conveyor belt, thus:

$$F_s = G_\gamma \cdot \cos\alpha \tag{16}$$

where:

F_s is the supporting force, N; G_γ is the weight of the kelp and rope, N;

α is the inclination angle of the hauling platform, (°).

Since the rope is a flexible body, the point of force application is assumed to be at its midpoint. When the included angle between the seedling rope ends is β, the normal force acting on a single side locking device is:

$$F_n = 2F_s \cdot \cos\frac{\beta}{2} \quad (17)$$

where: F_n is the normal force acting on a single side locking device, N; β is the included angle of the seedling rope, (°).

Since the pusher must overcome the friction between the seedling rope and the arc-shaped groove of the locking device to disengage the rope, and there is an inclination angle between the seedling rope and the locking device, then the frictional force that the pusher needs to overcome is:

$$f = \mu \cdot F_n \cdot \cos\varphi \quad (18)$$

where: μ is the coefficient of friction between the seedling rope and the locking device, taken as 0.3, φ is the angle between the seedling rope and the locking device, (°).

Since the pusher mechanism is designed based on the involute curve of the locking device, the distance from the pusher's rotation axis to the point of force application is considered the moment arm, and the required torque can be calculated accordingly:

$$M = F_p \cdot r_m \quad (19)$$

where:

M is the required rotational torque, Nm;

r_m is the moment arm length from the pusher's rotation axis to the point of force application, m.

Control System Design

Hardware Design of the Control System

The control system is centered on the Delta DVP-ES2 series PLC (Programmable Logic Controller), and its hardware configuration is shown in Figure 9, mainly consisting of a Delta PLC controller, a 24V switching power supply, a Pufeide driver, a ball screw, a stepper motor, a stepper electric push rod, a metal sensing switch, and a proximity sensor.

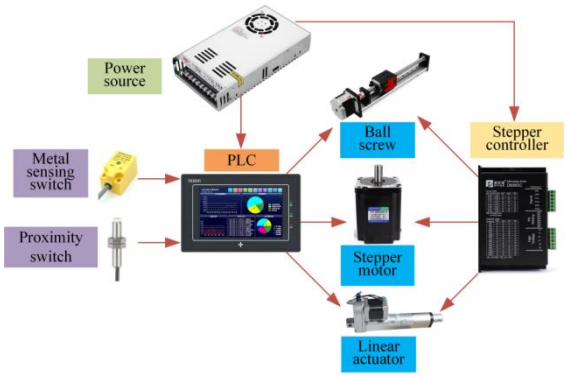

Fig. 9 - Hardware configuration diagram of the control system

The power supply required by each component in the control system is provided by a switching power supply, and a proximity sensor is used to determine whether the locking device is correctly positioned, with its feedback signal sent to the PLC controller for logical evaluation *(Xin et al., 2018)*. A metal sensing switch is used to detect whether the quick-release blocking device has reached the designated position, and the sensing signal triggers subsequent actions of the disengagement device. The ball screw assembly, driven by the motor, enables the forward and backward reciprocating movement of the quick-release blocking plate, thereby controlling the engagement and release of the quick-release structure. The stepper electric push rod is used to apply a pushing force, creating the necessary compressive force between the quick-release locking device and the blocking plate, thereby enabling automatic unlocking. All actuators are current-regulated and pulse-controlled by the Pufeide stepper motor driver, achieving precise control of displacement and speed. The PLC controller is programmed with predefined logic, which makes real-time decisions based on sensor input signals, and controls the timing of motor and push rod operations. The control panel provides parameter setting and operation status monitoring via a human-machine interface (HMI), facilitating on-site commissioning and operation.

Program Design of the Control System

Based on the operation process of rapid disengagement of kelp seedling ropes, a complete automatic control program was developed for the control system. The overall control flow of the system is illustrated in Figure 10. The program is coordinated by a PLC controller to manage the operation of all modules, in conjunction with hardware components including the electric push rod, motor, proximity sensor, metal sensing switch, and magnetic attraction module, to achieve precise unlocking of the locking device and the disengagement of the seedling rope. After initialization, the system automatically resets all components and awaits operation commands via the user interface to begin the process.

The locking device moves with the haulage rope into the flared guiding slot, where the magnetic module is activated to strongly attract the locking device and stabilize its posture. Subsequently, the electric push rod drives the locking device toward the blocking plate, until the proximity sensor detects contact between the locking device and the blocking plate, indicating that the unlocking has been completed. The PLC then drives the pusher configuration to rotate. After the rope is disengaged, the control system reverses the movement of the lead screw, moving the disengagement zone backward. Throughout the entire control process, the PLC continuously monitors the status of all sensors, and the execution completion signals, enabling precise and coordinated control, improving the efficiency and success rate of the disengagement operation.

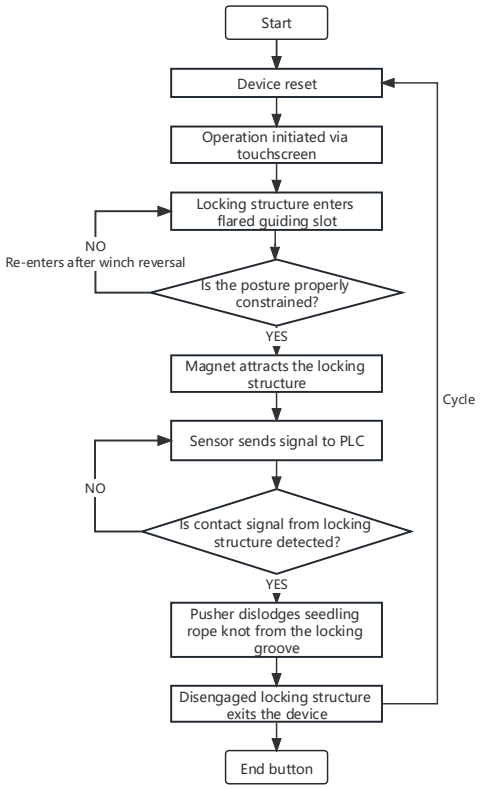

Fig. 10 - Control system flowchart.

EXPERIMENT AND ANALYSIS

Experimental Method

(a) (b)

Fig. 11 - Bench test diagram

To verify the reliability of the PLC-controlled rapid disengagement device for kelp seedling ropes under various operating conditions, key components were fabricated using 3D printing, and a bench-scale testing system was constructed. The disengagement success rate was used as the evaluation index, and an orthogonal experiment was conducted using three variables—guiding slot clearance, haulage rope speed, and pusher length to optimize structural parameters and enhance operational stability. Guiding slot clearance directly affects posture constraints and frictional behavior of the locking device; therefore, its lower limit was set slightly greater than the suspension rope diameter, and the upper limit was defined by effective posture restriction. Based on structural considerations, clearance levels were set from 8 to 24 mm.

Haulage rope speed determines the effectiveness of positioning and rope disengagement. According to the coordination between vessel speed and disengagement speed during harvesting, the range was set to 20-100 mm/s. Pusher length, which affects disengagement effectiveness, was set between 40 and 50 mm.

Orthogonal Experiment and Verification

Given that the performance of the rapid disengagement device is the result of multiple interacting factors and based on the results of the previously conducted single-factor experiments, an orthogonal optimization experiment was conducted with guiding slot clearance, haulage rope speed, and pusher length as experimental factors, and the factor level coding table is presented in Table 1.

Table 1

Coding table of test factors

Level	Factor		
	Guide slot gap a / mm	Speed of rope movement b / mm·s^{-1}	Length of dial finger c / mm
-1	10	20	40
0	14	40	45
1	18	60	50

The disengagement success rate was used as the evaluation index for assessing the performance of the disengagement device, and the experimental design and results are shown in Table 2.

For each test condition, 30 repeated trials were conducted, recording whether the seedling rope could be smoothly disengaged from the locking groove after unlocking, and the number of successful cases was counted to calculate the success rate of disengagement.

$$P = \frac{n}{n_0} \cdot 100\% \tag{20}$$

Where: P is the disengagement success rate, n is the number of successful disengagements, n_0 is the total number of trials.

Table 2

Design and results of simulation test

Test number	Guide slot gap a / mm	Speed of rope movement b / mm·s^{-1}	Length of dial finger c / mm	Success rate of disengagement R1 / %
1	14	60	40	70
2	10	40	50	66.67
3	14	40	45	96.67
4	14	60	50	50
5	18	40	40	66.67
6	14	40	45	93.33
7	10	40	40	73.33
8	18	20	45	83.33
9	14	20	40	86.67
10	18	40	50	53.33
11	10	60	45	70
12	14	40	45	96.67
13	14	40	45	86.67
14	14	40	45	96.67
15	18	60	45	50
16	10	20	45	80
17	14	20	50	83.33

Analysis of Experimental Results

Based on the experimental results in Table 2, an analysis of variance (ANOVA) was conducted on the disengagement success rate, and the results are shown in Table 3. The regression equation for the disengagement success rate is expressed as follows:

$$R_1 = 94 - 4.58a - 11.67b - 5.42c - 5.83ab - 1.67ac - 4.16bc - 15.33a^2 - 7.83b^2 - 13.67c^2 \quad (21)$$

Table 3

Analysis of variance for the regression model

Index	Source	Sum of squares	Degree of freedom	Mean square	F-value	P-value
Success rate of disengagement	Model	3960.92	9	440.10	36.72	< 0.0001**
	a	168.09	1	168.09	14.02	0.0072**
	b	1088.81	1	1088.81	90.84	< 0.0001**
	c	234.79	1	234.79	19.59	0.0031**
	ab	136.07	1	136.07	11.35	0.0119*
	ac	11.16	1	11.16	0.9307	0.3668
	bc	69.39	1	69.39	5.79	0.0470*
	a^2	990.12	1	990.12	82.60	< 0.0001**
	b^2	258.46	1	258.46	21.56	0.0024**
	c^2	786.50	1	786.50	65.61	< 0.0001**
	Residual	83.91	7	11.99		
	Lack of Fit	8.34	3	2.78	0.1472	0.9263
	Pure Error	75.56	4	18.89		
	Cor Total	4044.82	16			

Note :**indicates P≤0.01 (highly significant), *indicates P≤0.05 (significant).

As shown in Table 3, the P-value for the disengagement success rate model is less than 0.01, indicating that the regression model is highly significant. The coefficient of determination (R^2) is 0.9793, indicating that model R_1 explains most of the variability in the response value. The lack of fit P-value is 0.9263, which is greater than 0.05, suggesting that the experimental error is small and the model is reasonable, and that model R_1 can be used to predict the trend of disengagement success rate. The influence of operating parameters on disengagement success rate can be assessed based on the F-values, the influence of operating parameters on disengagement success rate can be assessed based on the F-values, and the order of significance of the factors is as follows: haulage rope speed > pusher length > guiding slot clearance.

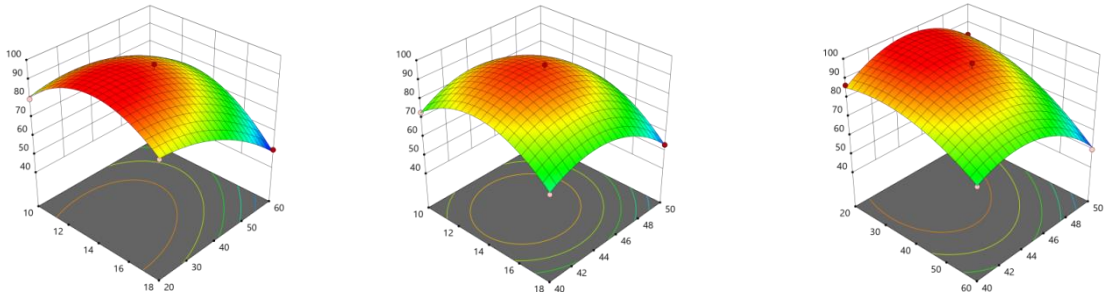

(a) (b) (c)

Fig. 12 - Response surface analysis of significant interaction terms on disengagement success rate

Parameter Optimization

To determine the optimal operating parameter combination for the rapid disengagement device, the Optimization module built into the Design-Expert software was used, to optimize the regression model. Considering both operating efficiency and effectiveness, the disengagement success rate was set as the objective to be maximized, with constraints applied to the objective function as shown in Equation (22).

$$\begin{cases} \max R_1(a,b,c) \\ \text{s.t.} \begin{cases} 10\text{mm} \le a \le 14\text{mm} \\ 20\text{mm/s} \le b \le 60\text{mm/s} \\ 40\text{mm} \le c \le 50\text{mm} \end{cases} \end{cases} \quad (22)$$

Based on the defined constraints, the objective function was optimized, resulting in the optimal parameter combination for the rapid disengagement device: guiding slot clearance of 14 mm, haulage rope speed of 40 mm/s, and pusher length of 45 mm, with a predicted disengagement success rate of 96.67% under the optimal parameters.

To verify the predictive accuracy of the response models and the overall performance of the prototype under the optimal parameter combination, a validation test was conducted, to confirm the accuracy of the regression model and the reliability of the optimization results derived from the orthogonal experiment. The operating parameters were: guiding slot clearance of 14 mm, haulage rope speed of 40 mm/s, and pusher length of 45 mm, with five repeated trials conducted under these conditions and the results averaged, the test results are shown in Table 7.

Table 7

Effect of haulage rope speed on disengagement success rate

Items	Experimental values		Predicted values
Success rate of disengagement	1	96.67	96.67
	2	93.33	
	3	90	
	4	96.67	
	5	96.67	

CONCLUSIONS

Based on the posture variation and force characteristics of the locking device during the disengagement of kelp seedling ropes, a rapid disengagement device was developed, consisting of a flared guiding slot for constraint, a magnet for positioning, an electric push rod for unlocking, and a pusher for rope disengagement. Three key structural parameters were identified: guiding slot clearance, haulage rope speed, and pusher length. The structural design was used to ensure both stable operation of the locking device and smooth release of the seedling rope, offering good operability and adaptability.

A response surface model was established, an orthogonal experiment was conducted, and a second-order polynomial regression model was developed using Design-Expert software. The analysis revealed that the influence of the three factors on disengagement success rate followed the order: haulage rope speed > pusher length > guiding slot clearance, resulting in the optimal parameter combination: guiding slot clearance of 14 mm, haulage rope speed of 40 mm/s, and pusher length of 45 mm. Under these parameters, the quick-release device operated stably with a high unlocking success rate, and the predicted disengagement success rate was 96.67%.

The research results provide a theoretical basis and data support for the structural optimization and parameter selection of the rapid disengagement mechanism, laying a foundation for the subsequent realization of automatic separation, intelligent control, and efficient harvesting of kelp seedling ropes.

ACKNOWLEDGEMENT

This research was funded by the Key R&D Program Project in Shandong Province, grant number 2022CXGC020410.

REFERENCES

[1] Bak, U.G., Mols-Mortensen, A., Gregersen, O. (2018). Production method and cost of commercial-scale offshore cultivation of kelp in the Faroe Islands using multiple partial harvesting. *Algal Research*, Vol.33, pp.36-47. https://doi.org/10.1016/j.algal.2018.05.001

[2] Branch, R., Rose, D., Grear, M., Briggs, C., Rollano, F.T. (2023). Powering the Blue Economy: Marine Energy at Kelp Farm Sites. *Marine Technology Society Journal*, Vol.57, no.4, pp.6-14.

[3] Forbes, H., Shelamoff, V., Visch, W., Layton, C. (2022). Farms and forests: evaluating the biodiversity benefits of kelp aquaculture. *Journal of Applied Phycology*, Vol.34, no.6, pp.3059-3067. https://doi.org/10.1007/s10811-022-02822-y

[4] Grebe, G.S., Byron, C.J., Gelais, A.S., Kotowicz, D. M., Olson, T.K. (2019). An ecosystem approach to kelp aquaculture in the Americas and Europe. *Aquaculture Reports*, Vol.15.

[5] Hewei, L., Bin, H. (2020). Research on bionic kelp harvesting device (仿生型海带采收装置的研究). *Journal of Fisheries Research*, Vol.42, no.5, pp.445-452.

[6] Mac Monagail, M., Cornish, L., Morrison, L., Araújo, R., Critchley, A.T. (2017). Sustainable harvesting of wild seaweed resources. *European Journal of Phycology*, Vol.52, no.4, pp.371-390. https://doi.org/10.1080/09670262.2017.1365273

[7] Min, Z., Gang, L., Yao, Y., Mei, J., Tao, J. (2023). Design and Parameter Optimization of Variable Speed Reel for Oilseed Rape Combine Harvester. *Agriculture*, Vol.13, no.8. https://doi.org/10.3390/agriculture13081521

[8] Peteiro, C., Sánchez, N., Martínez, B. (2016). Mariculture of the Asian kelp Undaria pinnatifida and the native kelp Saccharina latissima along the Atlantic coast of Southern Europe: An overview. *Algal Research*, Vol.15, pp.9-23.

[9] Tao, J., Yang, H., Longfei, L., Ye, Z., Zhixin, C., Meng, Y. (2022). Design and experiment of a new mode of mechanized harvesting of raft cultured kelp. *Aquacultural Engineering*, Vol.99. https://doi.org/10.1016/j.aquaeng.2022.102289

[10] Tao, J., Zhixin, C., Ye, Z., Yang, H., Haishen, Z., Yongming, T., Wei, Y. (2020). Design of kelp harvest and transfer device (海带收获转运装置设计). *Fishery modernization*, Vol.47, no.1, pp.16-23.

[11] Tullberg, R.M., Nguyen, H.P., Wang, C.M. (2022). Review of the Status and Developments in Seaweed Farming Infrastructure. *Journal of Marine Science and Engineering*, Vol.10, no.10. https://doi.org/10.3390/jmse10101447

[12] Vea, J., Ask, E. (2010). Creating a sustainable commercial harvest of *Laminaria hyperborea*, in Norway. *Journal of Applied Phycology*, Vol.23, no.3, pp.489-494. https://doi.org/10.1007/s10811-010-9610-y

[13] Xin, J., Kaixuan, Z., Jiangtao, J., Xinwu, D., Hao, M., Zhaomei, Q. (2018). Design and implementation of Intelligent transplanting system based on photoelectric sensor and PLC. *Future Generation Computer Systems*, Vol.88, pp.127-139. https://doi.org/10.1016/j.future.2018.05.034

[14] Yiren, Q., Yaoming, L., Yi, Y., Lizhang, X., Zheng, M. (2021). Development and experiments on reel with improved tine trajectory for harvesting oilseed rape. *Biosystems Engineering*, Vol.206, pp.19-31. https://doi.org/10.1016/j.biosystemseng.2021.02.016

[15] Yongming, T., Shangyou, L., Zhixin, C. (2020). Research on integrated specialized ship for kelp harvesting, classifying and grading. *Aquacultural Engineering*, Vol.91. https://doi.org/10.1016/j.aquaeng.2020.102121

[16] Yongming, T., Zhixin, C., Shupo, C., Shangyou, L., Tao, J. (2018). Design of automatic drafting and hanging kelp harvesting vessel (自动拖拽转挂式海带采收船的设计). *Fishery modernization*, Vol.45, vol.5, 69-74.

[17] Zimin, H., Tifeng, S., Jie, Z., Quansheng, Z., Critchley, A. T., Choi, H. G., Yotsukura, N., Fuli, L., & Delin, D. (2021). Kelp aquaculture in China: a retrospective and future prospects. Reviews in Aquaculture, Vol.13, no.3, pp.1324-1351. https://doi.org/10.1111/raq.12524

[18] Zimin, H., Tifeng, S., Quansheng, Z., Fuli, L., Jueterbock, A., Gaoge, W., Zhongmin, S., Xiangyu, W., Weizhou, C., Critchley, A.T., Naihao, Y. (2023). Kelp breeding in China: Challenges and opportunities for solutions. *Reviews in Aquaculture*, Vol.16, no.2, pp.855-871. https://doi.org/10.1111/raq.12871

[19] Zongyu, C., Yang, Z., Zhongqiang, Z., Rong, W., Zhixin, Z. (2018). Development status of the raft—cultivation harvesting devices for kelp (筏式养殖海带收获装置的发展现状). *Fishery modernization*, Vol.45, no.1, pp.40-48.